fishes

MDPI

Article

Broadband Scattering Characteristic Quantization Technique for Single Fish Based on a Split-Beam Echosounder

Qiuming Ai [1,2], Haisen Li [1,3,4,*], Jin Yao [1], Chao Li [5] and Jiangping Tao [1]

[1] College of Underwater Acoustic Engineering, Harbin Engineering University, Harbin 150001, China; kiana@hrbeu.edu.cn (Q.A.); yaojin1982@hrbeu.edu.cn (J.Y.); jptao@mail.ihe.ac.cn (J.T.)
[2] Nanhai Institute, Harbin Engineering University, Sanya 572024, China
[3] National Key Laboratory of Underwater Acoustic Technology, Harbin Engineering University, Harbin 150001, China
[4] Key Laboratory of Marine Information Acquisition and Security, Harbin Engineering University, Ministry of Industry and Information Technology, Harbin 150001, China
[5] SANYA Offshore Oil & Gas Research Institute, Northeast Petroleum University, Sanya 572024, China; chaoli@hrbeu.edu.cn
* Correspondence: hsenli@126.com

Abstract: The utilization of broadband quantization data increases the possibility of practical applications for fish target recognition based on the acoustic scattering theory. However, the quantification of broadband data is more complex than that of narrowband systems, requiring consideration of the broadband characteristics of split-beam transducers, seawater absorption, and circuits. This paper elucidates the scatterer acoustic field equation, transducer power equation, and signal processing flow in split-beam broadband quantization technology for engineering applications. A broadband calculation model based on transducer parameters is proposed to enhance the generalization ability of broadband quantization technology to different types of sonar. The classical echo integration method is combined with Fourier transform to meet the requirements of target strength (TS) estimation under broadband signals. This paper includes a series of experiments to prove the rationality and effectiveness of the method. The results demonstrate that the provided calculation model can more accurately reflect the backscattering characteristics of the scatterer, but certain errors remain. This article analyzes the sources of errors and validates the effectiveness of the new TS calculation method.

Keywords: split-beam echosounder; broadband technology; target strength; Helmholtz-Thevenin circuit; echo integration; Fourier transform; fisheries acoustics

Key Contribution: By combining scatterer acoustic field theory, an equivalent circuit for the transducer, and digital signal processing technology, the broadband TS calculation principle for fish is derived in detail, and a new broadband TS estimation method is proposed.

check for updates

Citation: Ai, Q.; Li, H.; Yao, J.; Li, C.; Tao, J. Broadband Scattering Characteristic Quantization Technique for Single Fish Based on a Split-Beam Echosounder. *Fishes* **2024**, *9*, 12. https://doi.org/10.3390/fishes9010012

Academic Editors: Jianfeng Tong, Yong Tang and Tohru Mukai

Received: 17 November 2023
Revised: 22 December 2023
Accepted: 24 December 2023
Published: 27 December 2023

1. Introduction

Acoustic detection technology based on scientific echosounders is widely used in the field of fishery resource investigation [1–9]. This type of echosounder performs vertical or horizontal detection underwater by transmitting and receiving acoustic waves [1]. The sound pressure is converted to an electrical signal by the transducer and amplified by the circuits, and echo integration is used to analyze the target scattering characteristics [2–8]. The split-beam method is an improvement based on single-beam technology [9] and it is one of the mainstream methods for measuring the backscattering cross-section of marine organisms [5,7]. The principle is that by splitting the receiving plane array into four quadrants [2,3,5–7], and then employing the principle of time delay positioning [10], Assuming that the values of the beam pattern at all angles in space are known, the influence of the beam pattern can be removed based on the calculated target position [2,5–7]. In principle, the TS of the detected

object can be calculated through a single echo calculation. Simrad EK500 and EK60 are narrow-band split-beam echosounders commonly used in fishery acoustic surveys [5,11–13]. Among these, the EK500 operation manual proposes TS calculation based on the power budget equation. The formula is deformed based on the radar equations, and the TS value is derived, based on the spherical scattering cross section [14]. The spherical scattering cross section corresponds to the radar scattering cross section in the radar equation [15,16], which needs to be divided by the spatial angle to convert it into the acoustic backscattering cross section [17]. Lunde derived the calculation formulas of narrow-band devices such as EK500 and EK 60 in detail by using acoustic models [11]. Although the formula is reasonable, the definition of transducer array gain G is too complex. Most calculation methods rely on equipment and calibration parameters [1,3,5,6,11–13] and do not mention the processing of the beam pattern. EK80 is currently one of the most mainstream broadband split-beam echo sounders and is considered to be the next-generation device to replace EK60 [12,13]. Most broadband split-beam research is based on this assumption. Lars Nonboe Andersen provided a comprehensive introduction to the quantitative processing of broadband data using the EK80 broadband system [7]. The TS calculation formula was derived based on Lunde's formula, which lacks an analysis of the processing of the beam pattern under the broadband, and the transducer gain parameter G in the equation relies on the broadband calibration of the standard scattering sphere [7,12,13,18]. The calibration of broadband equipment is more complicated. Due to the multiple resonances of the sphere within the broadband [19], a rigid sphere of specific material is generally selected as a reference, ensuring the effectiveness of the calibration of the broadband equipment [20]. Dezhang Chu also stated that during the process of designing calibration experiments for broadband systems, calibration is essential in order to obtain high-quality acoustic data [21]. Broadband systems bring more information to fishery acoustics [7,12,22], but data processing is complex and unclear. Although most of the formulas have been proven to be reasonable [7,11], the current calculation methods for broadband systems do not provide a complete acoustic scheme. An over-reliance on calibration information makes it impossible to obtain a valid absolute estimate of the TS value in some scenarios in which there are no standard scatterers. To combine broadband technology with split-beam echo sounders, this article takes the scientific echosounder EK80 as the research object and carries out the following research.

The main purpose of this article is to:

1. Derive the radiation and single target scattering model of the circular piston transducer under far-field conditions. The calculation formula for the backscattering cross section under a single target is given by combining the Helmholtz-Thevenin equivalent circuits model and the acoustic parameters of the transducer.
2. Establishes a processing flow for broadband data under a single target and derives the echo integration under broadband based on Fourier transform.
3. Using EK80 as the experimental object, this research designs several transducer parameter test experiments and a copper ball TS measurement experiment to compare and verify the accuracy of the calculation model.

2. Materials and Methods

2.1. Single-Target Scattering Model and Backscattering Cross Section in the Far Field

The derivation is based on the free field. Both the scatterer and the transducer satisfy far-field conditions, and the finite amplitude effect is ignored [23,24]. The transducer is a transceiver and satisfies reciprocity.

Figure 1 shows a simplified detection scenario in a typical monostatic configuration, where the transducer is a circular piston transducer, and the spherical coordinate system is established based on the equivalent acoustic center of the transducer plane. Considering

absorption loss, the sound pressure p of the reference point (r, θ) in the sound field is shown in Equation (1) [25].

$$p(r,\theta) = j\rho_w c_w k u_0 a^2 e^{-jkr} \frac{10^{-\alpha r/20}}{r} \frac{J_1(ka\sin(\theta))}{ka\sin(\theta)} \tag{1}$$

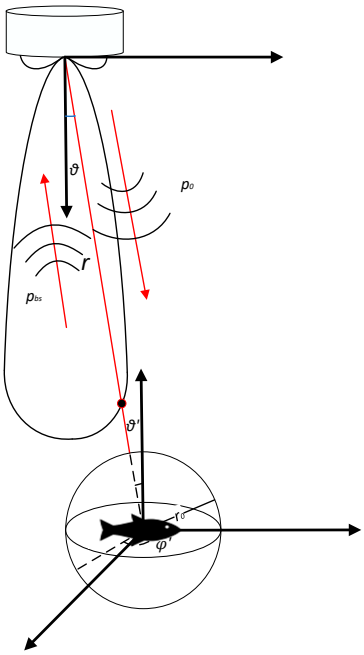

Figure 1. Schematic of a single fish backscatter acoustic system, with an electroacoustic transducer as the transmitter and receiver of the acoustic signal.

Among these, ρ_w is the density of water, c_w is the sound velocity of water, k is the wave number, u_0 is the particle vibration velocity, a is the diameter of the transducer, α Is the absorption coefficient of the medium, and J_1 is the first-order Bessel function. For the convenience of subsequent analysis, we take the reference distance r_0 and set the sound pressure amplitude as p_0, ignoring the time-harmonic factor e^{-jkr}, to obtain the radiation sound pressure amplitude of the transducer in the sound field as shown in Equation (2) [24], Equation (3) is the expression of the beam pattern [25].

$$|p(r,\theta)| = p_0 \frac{10^{-\alpha r/20}}{r} b(\theta) \tag{2}$$

$$b(\theta) = \frac{J_1(ka\,\sin(\theta))}{ka\,\sin(\theta)} \tag{3}$$

It is assumed that the object in Figure 1 is a single object of any shape or material, or a collection of various types of objects of different types of materials. The overall volume is limited to meet the requirements that it should be smaller than the first Fresnel zone of the sound beam, which can be completely engulfed by the sound beam. Objects that meet these requirements can be considered as a single target for analysis, and their scattering characteristics can be regarded as scattering from point-like objects [17]. It is assumed that the far field conditions for point scattering are met. Taking the backscattered sound pressure amplitude p_{bs0} at the reference distance r_0 as the initial value before the spherical diffusion of the sound pressure, the scattered wave is received by the transducer in the

form of a plane wave. Then the sound pressure p_{bs} generated by the scatterer at the sound center of the transducer can be obtained, as shown in Equation (4).

$$p_{bs} = \frac{p_{bs0}}{r} 10^{-\alpha r/20} \tag{4}$$

Based on the physical definition of the backscattering cross-section mentioned previously [26], Equation (5) can be obtained.

$$\frac{p_{bs0}}{|p(r,\theta)|} = \frac{\sqrt{\sigma_{bs}}}{r_0} \tag{5}$$

According to Equations (2)–(5), the final amplitude of sound pressure generated on the surface of the transducer can be obtained using Equation (6).

$$p_{bs} = p_{bs0} \frac{10^{-\alpha r/20}}{r} = p_0 \frac{10^{-\alpha r/10}}{r^2} b(\theta) \sqrt{\sigma_{bs}} \tag{6}$$

To calculate the backscattering cross-section of the target, Equation (6) is deformed, and the backscattering cross-section with respect to the square ratio of the sound pressure amplitude is obtained, as shown in Equation (7).

$$\sigma_{bs} = \left(\frac{p_{bs}}{p_0} \right)^2 \frac{r^4 10^{-2\alpha r/10}}{b^2(\theta)} \tag{7}$$

Equation (7) is then converted into TS [17,26], as shown in Equation (8).

$$TS = 20\log\left(p_{bs}\right) - 20\log\left(p_0\right) + 40\log(r) + 2\alpha r - 20\log\left(b(\theta)\right) \tag{8}$$

Theoretically, by measuring the emission sound pressure value and the scattering sound pressure value, calculating the spatial coordinates of the scattering target, and finally combining them with absorption loss of the medium, the backscattering cross section can be acquired, and then the TS can be obtained. In the next section, the connection between the sound pressure amplitude and the circuit system will be introduced and the theoretical calculation equation of the TS in broadband scenarios will be provided.

All the symbols and variables in Section 2.1 are presented in Table A1 in Appendix A, containing units and a brief description.

2.2. Equivalent Model of Helmholtz-Thevenin Circuit for Transducers

In order to obtain the relationship between the ratio of sound pressure to the circuit, we must focus on describing the conversion performance of the acoustic and electrical signals of the transducer, which is defined as the sensitivity of the transducer. It is assumed that the transducer satisfies reciprocity, is passive, that the voltage it transmits and receives is linear in relation to the sound pressure, and that the free-field condition is satisfied. The transmitting sensitivity s_u and receiving sensitivity m_u of the transducer are defined by voltage as follows [27,28]:

$$s_u = \frac{p_0}{V_T}, \; m_u = \frac{V_o}{p_{ax}} \tag{9}$$

where p_0 is the axial sound pressure value generated at the reference point at V_T voltage, and V_o is the open-circuit voltage generated at the equivalent axial sound pressure p_{ax}. The non-axial incident sound pressure will be affected by the beampattern of the transducer's receiving array. According to the reciprocity of the transducer [11], the beampattern when transmitting is consistent with the beampattern function expression when receiving, so the axial sound pressure amplitude is equivalent to

$$p_{ax} = p_{bs} b(\theta) \tag{10}$$

According to the Equation (10), the formula for the backscattering cross-section can be expressed with the transmitting sensitivity, receiving sensitivity, beam pattern, and sampled voltage, as shown in Equation (11).

$$\sigma_{bs} = \left(\frac{V_o}{s_u m_u V_T}\right)^2 \frac{r^4 10^{-2\alpha r/10}}{b^4(\theta)} \tag{11}$$

Usually, the transducer works together with the matching circuit in the receiving state. In order to obtain the voltage in Equation (11), it is necessary to combine the transducer and its matching circuit for analysis.

The left side of Figure 2 shows a simplified circuit when the transducer is in the transmitting state [5,7,11]. The equivalent impedance of the transducer is Z_T, in which the resistance R_T of the transducer is the real part of the impedance. The active power transmitted by the circuit can be expressed as Equation (12),

$$\Pi_T = \frac{|V_T|^2}{2|Z_T|^2} R_T \tag{12}$$

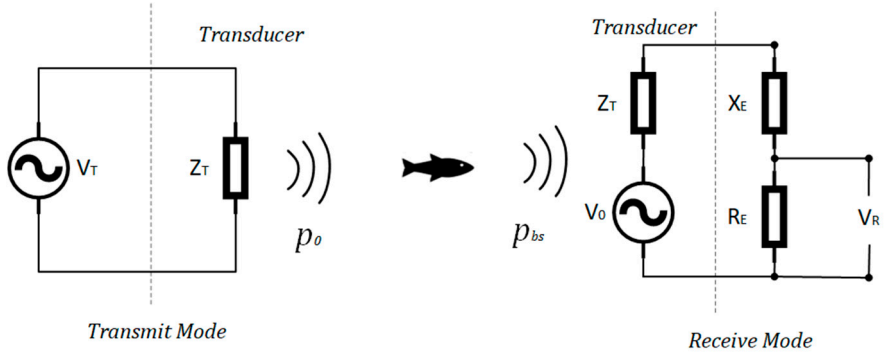

Figure 2. Helmholtz-Thevenin equivalent model for the transceiver circuit, in which the dotted line indicates the transducer. In the transmit mode, the transmit circuit can be regarded as a voltage source. In receiving mode, the voltage V_R across the resistor R_E of the matching circuit is sampled.

The transmit power can usually be measured using the power detection circuit. The amplitude of the transmit voltage obtained by deforming Equation (12) can be expressed as Equation (13).

$$V_T = \sqrt{\frac{2|Z_T|^2 \Pi_T}{R_T}} \tag{13}$$

To take the effect of non-ideal impedance into consideration when the transducer is receiving in the working state, the match circuit impedance $Z_E = R_E + iX_E$ needs to be considered as consistent [24]. The right side of Figure 2 shows the receiving equivalent circuit. The voltage collected on the equivalent resistance of the matching circuit is set to V_R. Then, the modulus value of the open-circuit voltage can be expressed as Equation (14):

$$V_o = \left|\frac{V_R}{R_E} \cdot (Z_T + Z_E)\right| \tag{14}$$

Usually, in order to ensure that the phase of the sampled electrical signal at each frequency is consistent with the phase of the received sound pressure, and to ensure that the time-domain waveform of the surface sound pressure of the transducer is consistent with the time-domain waveform of the electrical signal of the transducer under broadband signals, the matching circuit impedance Z_E is designed to minimize the impact caused by the reactance of the transducer [29]. Under ideal conditions, the parallel network of a

transducer that completes impedance matching can be regarded as pure resistance R_{TE}, and its open-circuit voltage can be expressed as Equation (15).

$$V_o = \left|\frac{V_R}{R_E}\right| R_{TE} \tag{15}$$

In summary, the backscattering cross section of the target is shown as Equation (16).

$$\sigma_{bs} = \frac{|V_R|^2 R_{TE}^2 R_T}{2s_u^2 m_u^2 |Z_T|^2 |R_E|^2 \Pi_T} \frac{r^4 10^{-2\alpha r/10}}{b^4(\theta)} \tag{16}$$

The impedance factor is defined as F_{Impe}, and the logarithms of the transmit and receive sensitivity are expressed as Su and Mu:

$$F_{Impe} = \frac{R_{TE}^2 R_T}{2|Z_T|^2 {R_E}^2} \tag{17}$$

$$Su = 20\log(s_u),\ Mu = 20\log(m_u) \tag{18}$$

Combining Equations (8) and (16)–(18), the TS can be obtained as shown in Equation (19):

$$TS = 20\log(V_R) + 10\log\left(F_{Impe}\right) - 10\log(\Pi_T) - Su - Mu + 40\log(r) + 2\alpha r - 40\log(b(\theta)) \tag{19}$$

In the actual measurement process, the impedance factor can be calculated by measuring the impedance of the transducer and the impedance of the matching circuit. The receiving sensitivity and transmitting sensitivity of the transducer are obtained by measuring the sound pressure at the acoustic axis of the specific transmitting and receiving circuit, using an oscilloscope and another transducer [30]. These parameters are usually provided in the transducer's parameter manual. The beam pattern function can be obtained by measuring the echo level of a standard metal ball at different angles [5], or by using a standard sound source [6] and fitting the obtained data through polynomial fitting.

Under a broadband signal, frequency variables can be introduced into the above equations, and considering the difference in the transducer beam pattern at different frequencies, the TS Equation (20) under broadband can be obtained,

$$\begin{array}{c} TS(f) = 20\log(V_R(f)) + 10\log\left(F_{Impe}(f)\right) - 10\log(\Pi_T(f)) - Su(f) - Mu(f) \\ +40\log(r) + 2\alpha(f)r - 40\log(b(\theta, \varphi, f)) \end{array} \tag{20}$$

This expression only provides theoretical support for the estimation of broadband TS. The echo integration method must be further derived in the actual calculation process.

All the symbols and variables in Section 2.2 are presented in Table A2 in Appendix A, containing units and a brief description.

2.3. Echo Integration and Voltage Estimation under Broadband

Ignoring nonlinear effects and assuming that the power value and sound intensity satisfy a proportional relationship, the echo integration $[tivs]$ under narrowband signals can be defined as the integral of the square of the received voltage over time [8,26]. For the convenience of analysis, it is assumed that the echo from the target has a constant amplitude A, frequency f, and phase φ, as shown in Equation (21).

$$v(t) = Acos(2\pi ft + \varphi) \tag{21}$$

Among these, $f = 1/T$, where T is the period of the narrowband signal. The reference resistance R_{ref} is set to 1 Ω. When the integration time τ is much larger than the period T,

due to the periodicity of the cosine signal, the power Π_{ref} can be derived from the echo integration, as shown in Equation (22).

$$\Pi_{ref} = \frac{[tivs]}{\tau R_{ref}} \approx \frac{1}{TR_{ref}} \int_T v^2(t)dt = \frac{A^2}{2} \tag{22}$$

Based on the calculated power and combined with the above equation, the TS of the fish can be calculated. Compared with the original signal, the echo from fish usually shows an expansion of pulse width and a fluctuation in amplitude over time [31–33]. During the calculation of echo integration, the original signal is windowed to obtain the average TS value of the target within the time window [11].

This can then be extended to broadband signals. Assuming that there is an ideal signal, $f_1 \sim f_m$ covers m frequency points, each signal duration is T, and T satisfies $T \gg 1/f_i$ for the frequencies of these signals to meet the periodic conditions derived in Equation (22), as shown in Equation (23).

$$s_{ideal}(t) = \begin{cases} A_1 cos(2\pi f_1 t + \varphi_1), & 0 < t \leq T \\ A_2 \cos(2\pi f_2 t + \varphi_2) & T < t \leq 2T \\ \vdots & \\ A_m cos(2\pi f_m t + \varphi_m), & (m-1)T < t \leq mT \end{cases} \tag{23}$$

Regardless of the pulse width change in the echo signal, when $limT \to 0$, the weighted average of each interval integral value over time can be obtained, as shown in Equation (24).

$$\frac{[tivs]}{T} = \lim_{T \to 0} \frac{A_i^2}{T} \left(\frac{sin4\pi f_i T}{4\pi f_i} + \frac{T}{2} \right) = \frac{A_i^2}{2} \tag{24}$$

In this way, the broadband echo integral is obtained under ideal condition. However, in actual engineering applications, the time window cannot be infinitely close to zero; therefore, it seems impossible to discretely sample the signal and perform echo integration for each frequency. According to Fourier transform properties, the rotation factor $e^{-j2\pi ft}$ of the Fourier transform can be used to estimate the amplitude squared of each frequency of the all the echoes at each frequency [34]. The Fourier integral of the above signal is expressed as Equation (25).

$$S(f) = \int_{mT} s_{ideal}(t) e^{-j2\pi ft} dt \tag{25}$$

When $f \neq f_i$, the integral value is 0 due to the orthogonality of the rotation factor and the signal, and when $f = f_i$, the integral value is shown as Equation (26).

$$S(f_i) = \frac{A_i T}{2} \frac{e^{j\varphi}}{j2\pi} \tag{26}$$

Taking its modulus, we can obtain an expression for the energy meaning of A_i.

$$A_i{}^2 = \frac{16\pi^2 |s(f_i) \cdot s^*(f_i)|}{T^2} \tag{27}$$

In engineering applications, an LFM signal is introduced as a broadband signal for analysis, and the expression of a typical LFM signal can be obtained in the real number domain [35], as shown in Equation (28):

$$s_{LFM} = Acos\left(2\pi f_0 t + \frac{\pi F}{T} t^2\right) = Acos(2\pi(f_0 + \frac{F}{2T}t)t) \tag{28}$$

Its equivalent frequency $f_e = f_0 + \frac{F}{2T}t$ and the duration of all signals in a narrow band can be regarded as an infinitely small value close to 0. The signals are time-varying in frequency, so the results obtained using the traditional echo integration method include the weighted average of all frequencies, which does not reflect the broadband characteristics of the target. The Fourier integral is used to estimate the amplitude of the broadband signal, and then the target broadband voltage response can be obtained.

In engineering, the received signals are sampled and quantified to obtain a discrete sequence of analog signals. Assume that the received LFM signal can be expressed as Equation (29), where A_n is the time domain response from the target.

$$x[n] = A_n \cos\left(\frac{2\pi f_n n}{f_s} + \varphi_n\right) \tag{29}$$

Since the transmitted signal is an LFM signal and the frequency is time-varying, for the convenience of analysis, the signal is subsequently converted into Fourier series form and subjected to Hilbert transform. Since the Fourier transform of LFM includes a Fresnel integral [36], the LFM frequency domain amplitude is instable, as shown in Figure 3; thus, DFT cannot be used directly to obtain the frequency domain response. In order to obtain the frequency domain response, this paper sets the ideal signal sent as the reference signal and the amplitude of the reference signal to 1 and then performs the same processing, as shown in Equations (30) and (31).

$$x_{complex}[n] = \sum_{i=1}^{N-1} A_i \exp\left(\frac{2\pi f_i n}{f_s} + \varphi_i\right) = A_n \exp\left(\frac{2\pi f_n n}{f_s} + \varphi_n\right) \tag{30}$$

$$x_{ref}[n] = \sum_{i=1}^{N-1} C_i \exp\left(\frac{2\pi f_i n}{f_s} + \varphi_i^{'}\right) = 1 \cdot \exp\left(\frac{2\pi f_n n}{f_s} + \varphi_n^{'}\right) \tag{31}$$

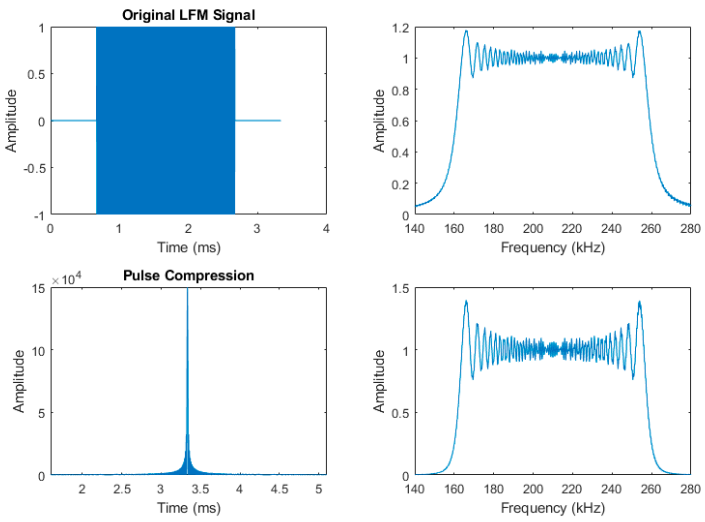

Figure 3. The upper left image shows the time domain form of the original LFM pulse, with a frequency range of 160 kHz~260 kHz, and the upper right image shows the frequency domain form of the original LFM pulse. The lower left image shows the signal after pulse compression. In order to show the changes in amplitude after pulse compression, the image was not normalized. The image on the lower right shows the spectrum after pulse compression processing. The amplitudes in the figure are reference values, without specific units.

A_i, C_i in the above formula are amplitudes in the form of a Fourier series, which are coupled with the sampling time and sampling frequency [37]; therefore, the time domain window length and sampling frequency of the received signal and the reference signal need to be consistent.

Usually, the reference signal is pulse compressed with the received signal and itself, as shown in Equations (32) and (33). This is performed to improve the signal-to-noise ratio [38]. The overall amplitude of the spectrum changes, and the pulse width in the time domain is compressed, as shown in Figure 3.

$$y_{pc} = x_{complex}[n] * conj(x_{ref}[-n]) \tag{32}$$

$$y_{ref} = x_{ref}[n] * conj(x_{ref}[-n]) \tag{33}$$

Attention: symbol * represents convolution operation in this paper.

The same reference signal is used for pulse compression. According to the convolution theorem and the principle of linear superposition [34], dividing the DFT results can eliminate the changes in spectrum amplitude caused by pulse compression. In this way, the amplitude ratio at each frequency can be obtained with Equation (34).

$$X_{responsor}(f) = \frac{DFT(y_{pc})}{DFT(y_{ref})} = \left| \sum_{i=1}^{N-1} \frac{A_i}{C_i} \delta(f - f_i) e^{j(\varphi_i - \varphi_i')} \right| \tag{34}$$

When the time domain amplitude of the reference signal is an arbitrary value, the l_2 norm of the reference signal can be used to normalize the time domain of the reference signal:

$$V_{norm}[n] = V_{ref}[n] \sqrt{\frac{N}{\left\| V_{ref}[n] \right\|_2}} \tag{35}$$

According to Equations (29)–(35), the broadband amplitude of the received voltage can be expressed by Equation (36):

$$V_R(f) = \frac{DFT\left[V_R[n] * conj\left(V_{ref}[-n]\right)\right]}{DFT\left[V_{ref}[n] * conj(V_{ref}[-n])\right]} \sqrt{\frac{\left\| V_{ref}[n] \right\|_2}{N}} \tag{36}$$

The overall process of calculating TS is summarized in Figure 4.

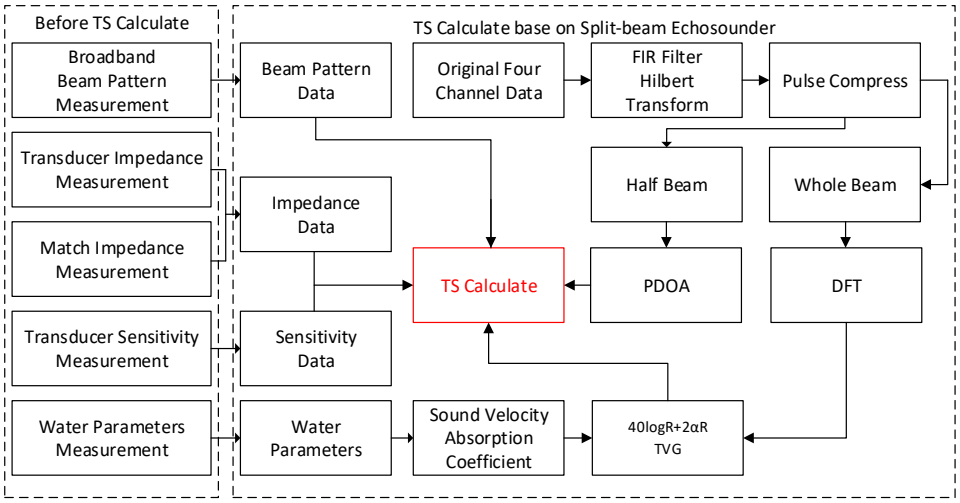

Figure 4. Overall data processing block diagram of a broadband split-beam echosounder. Before performing TS measurement, the data shown on the left side of the figure must be measured. The TS calculation includes a filtering algorithm, a positioning algorithm, and seawater absorption coefficient calculation. Due to space limitations, this is not explained in the text.

Among the calculations, the FIR filter is a commonly used noise reduction method [7,39]. The full beam is used for echo integration to obtain an estimate of TS. The phase difference of the half-beam is used to obtain the target position in the beam pattern, and the influence of the beam pattern on the full-beam TS estimation is removed [2,6,7]. In order to realize the above calculation process, experiments need to be designed to measure the above parameters.

All the symbols and variables in Section 2.3 are presented in Table A3 in Appendix A, containing units and a brief description.

3. Results

3.1. Transducer Sensitivity and Impedance Parameters

The experiment used the EK80 split beam echosounder system and selects the ES200-7C split beam broadband transducer with a nominal frequency of 200 kHz as the experimental object. The transducer manufacturer, Simrad AG (now Kongsberg Maritime AG), is located in Horten, Norway. Its parameters are shown in Table 1.

Table 1. Partial parameters of the ES200-7C transducer.

Parameters	Values
Transducer	ES200-7C
Nominal frequency (kHz)	200
Frequency range (kHz)	160~260
Beam type	Split-Beam
Nominal beam width (°)	7
Nominal Impedance (Ω)	75
Diameter (mm)	120

The sensitivity parameters and impedance under broadband were tested by the manufacturer [40], and the results are shown in Figure 5.

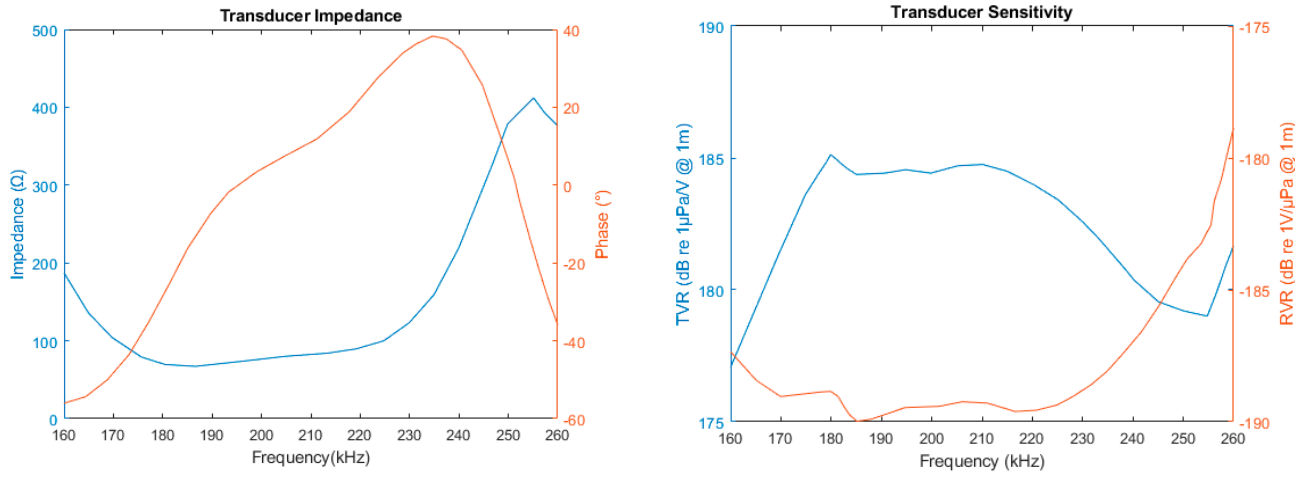

(**a**) (**b**)

Figure 5. (**a**) The impedance of the ES200-7C transducer; (**b**) the sensitivity of the ES200-7C, which includes receiving sensitivity and transmitting sensitivity.

The impedance of the ES200-7C transducer near the nominal frequency is about 75 Ω, and the impedance is significantly greater than 75 Ω at low and high frequencies far from the center frequency. The real and imaginary reactance of the impedance vary significantly with frequency. In a circuit, resistance dissipates energy, and reactance changes the phase of the signals at different frequencies. For the transmission circuit, digital signal processing technology can be used to perform amplitude compensation or phase compensation to maintain good phase and amplitude consistency in the final transmitted signal [41].For

the receiving circuit, a matching impedance network is built to reduce the impact of the nonlinear response of the transducer in the frequency domain, so that the sampled signal can be approximately proportional to the sound pressure value [29].

3.2. Matching Circuit Impedance Inversion Measurement

Since the broadband impedance data of the matching circuit inside the EK80 processor is not publicly available, a broadband sound source detection experiment must be designed to estimate the impedance of the EK80 matching circuit. This experiment was conducted in an anechoic pool with a length of 7 m, a width of 6 m, and a depth of 5 m. The sound source and standard hydrophones used the same model of hydrophones, and their parameters are shown in Table 2.

Table 2. Hydrophone parameters were used in the experiment.

Parameters	Values
Hydrophone type	Standard hydrophone
Model	TC4038-4
Effective frequency (MHz)	0.02~0.8
100 kHz receiving sensitivity (dB re 1V/μPa @1 m)	−238.09
300 kHz receiving Sensitivity (dB re 1V/μPa @1 m)	−237.81
Transmitting sensitivity (dB re 1μPa/V @1 m)	100~120
Horizontal directivity pattern (°)	360
Vertical directivity pattern (°)	120

The signal source uses DSG815, which can send AM, FM, and pulse signals in the frequency range of 9 kHz~1.5 GHz. The oscilloscope uses DS1102 with an analog bandwidth of 100 MHz, which can cover the bandwidth involved in this experiment.

The impedance can be calculated from the receiving sensitivity, sampling voltage value, and transducer impedance curve, as shown in Equation (37).

$$R_E = \frac{V_R R_T}{m_u p_r - V_R} \tag{37}$$

The parameters for the transmit signal and acquisition settings are shown in Table 3.

Table 3. Experimental emission signal parameters and oscilloscope sampling frequency.

Parameters	Values
Signal type	Linear FM
Pulse duration (ms)	1
Frequency range (kHz)	160~260
Transmitting amplitude (V)	3
Receiving amplifier gain (dB)	120
Oscilloscope sample frequency (MHz)	1

In order to estimate the equivalent impedance curve of the receiving matching circuit, the transducer was placed in the receiving state, and the EK80 system sampling voltage and standard hydrophone sound pressure were recorded. The experimental design is shown in Figure 6.

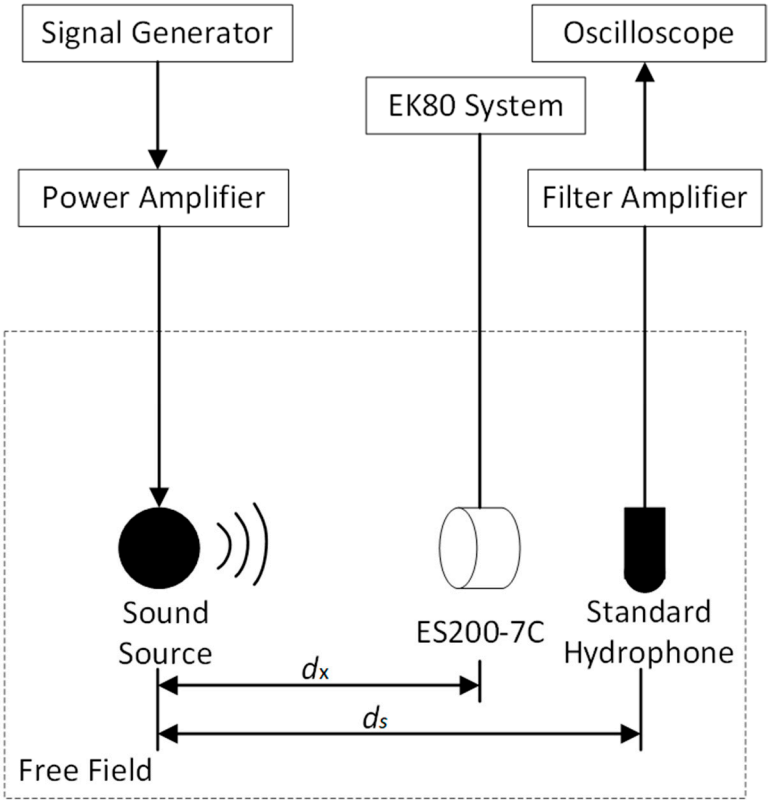

Figure 6. The dx and ds are set to 5 m, the sound source is in the axial direction of ES200-7C, and the hydrophone is placed near ES200-7C. Both are within the far-field range of the sound source. The sound pressure is kept consistent, according to the directivity of the sound source.

The sound source emits a broadband signal, and the transducer collects it using passive mode. The time domain voltage value sampled by the hydrophone is converted into the frequency domain sound pressure value $p_{ax}(f)$ using DFT and the sensitivity parameters, and then the voltage value sampled by the EK80, and the sound pressure value collected by the hydrophone are brought into the above formula. The calculated results are shown in Figure 7.

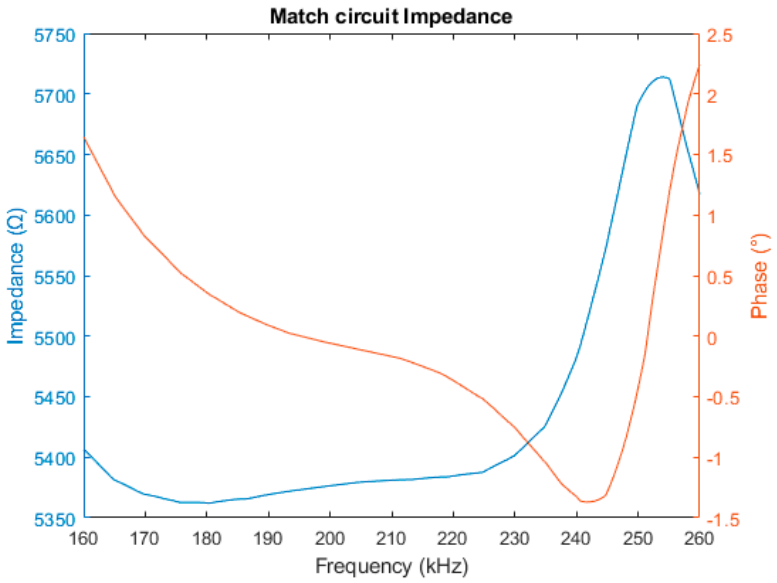

Figure 7. The matching impedance of the transducer calculated from the test data.

The impedance trend of the matching circuit is relatively consistent with that of the transducer. The changes in impedance near the frequency of 180 kHz to 220 kHz are small, and above 220 kHz the impedance changes significantly. Over most of the frequency range, the overall impedance value hovers in the range of 5350 to 5400 Ω.

3.3. Transducer Beam Pattern Measurement

Using the previous instrument, we continued to measure the beam pattern of the transducer in a broadband scenario, and the experimental design is shown in Figure 8.

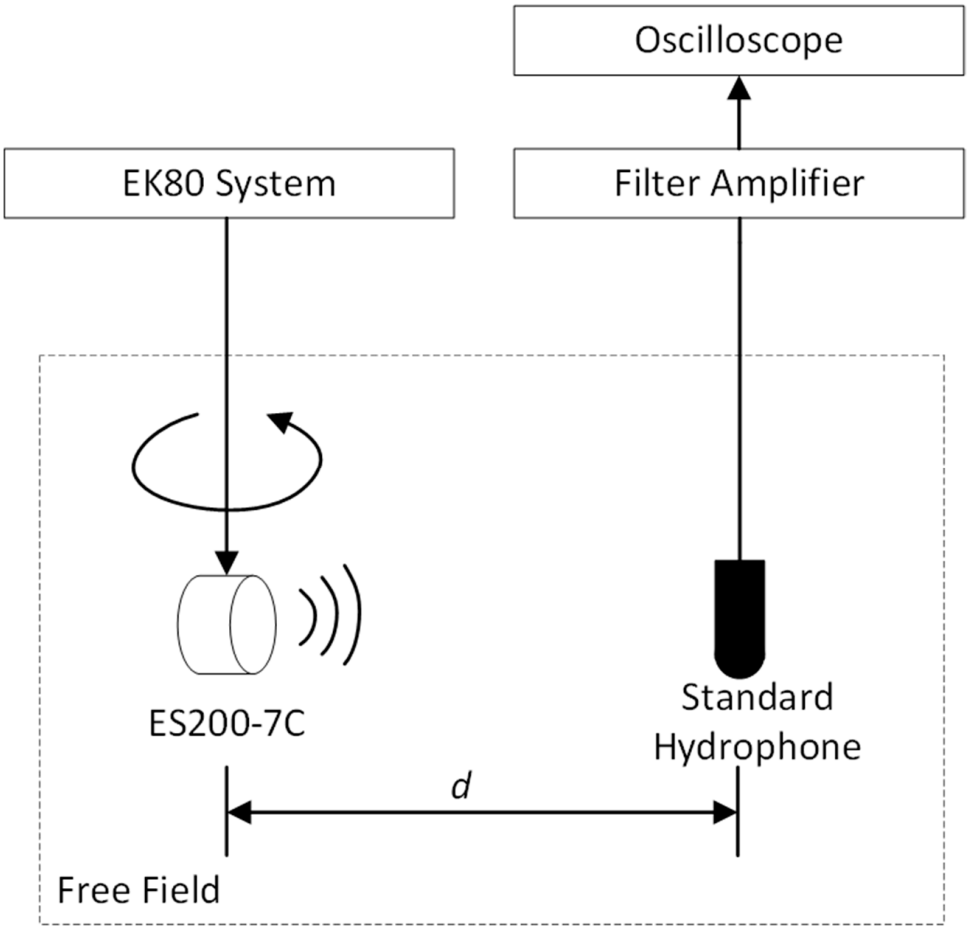

Figure 8. Beam pattern measurement experimental design. The distance d is set to 5 m to meet the far-field conditions of the transducer.

The transducer sends an LFM signal, the parameters are consistent with Table 3, and the hydrophone is used to record the sound pressure values at different angles. The received sound pressure values are subjected to discrete Fourier transform to obtain the sound pressure components at each angle. By taking the maximum point of the sound pressure ratio at the center frequency as the sound axis direction, the beam patterns at different frequencies can be obtained. The transducer is then rotated 90° and the measurement is repeated to obtain a beam pattern in the orthogonal direction.

The beam width measurement results are obtained from both directions, and the partial measurement results of the acoustic axis offset are shown in Table 4. The off-axis deviation in both directions can be calculated by the difference between the maximum value of the beam pattern and 0°, and the beam width is obtained from the difference between the left and right sides at −3 dB.

Table 4. Transducer beam pattern measurements result.

Frequency (kHz)	Alongship Beamwidth (°)	Athwartship Beamwidth (°)	Alongship Axis Bias (°)	Athwartship Axis Bias (°)
160	8.21	8.12	−0.04	0.05
165	7.82	7.76	−0.06	0.04
170	7.46	7.38	−0.05	0.06
175	7.12	7.08	−0.04	0.05
180	6.74	6.70	−0.05	0.04
185	6.47	6.46	−0.06	0.04
190	6.28	6.26	−0.06	0.06
195	6.14	6.08	−0.06	0.05
200	5.93	5.96	0	0
205	5.84	5.89	−0.04	0.02
210	5.66	5.70	0.01	0.03
215	5.46	5.58	0	0.04
220	5.40	5.51	0.02	0.02
225	5.36	5.44	0.01	0.03
230	5.30	5.31	0.01	0.03
235	5.18	5.18	0.03	0.02
240	5.10	5.13	0.03	0.02
245	5.05	5.07	0.01	0.02
250	4.98	5.01	0.04	0.04
255	4.92	4.96	0.02	0.01
260	4.85	4.92	0.03	0.02

During the measurement process, the beam pattern measurement results indicated a certain deviation in the acoustic axis. In the calculation the deviation parameter of the acoustic axis must be introduced, the measured beam pattern is polynomial fitted using the angle of two directions as independent variables, and the following beam compensation relationship is obtained [5], as shown in Equation (38), and Equation (39) describes the two variables.

$$b\left(\theta_{athwart}, \theta_{along}\right) = 10^{-0.0753*\left[(F_{athwart})^2+(F_{along})^2-0.18(F_{athwart})^2\cdot(F_{along})^2\right]} \tag{38}$$

$$F_{athwart} = \frac{\left|\theta_{athwart} - \theta_{athwart,bias}\right|}{\frac{\theta_{athwart,beamwidth}}{2}}, F_{along} = \frac{\left|\theta_{along} - \theta_{along,bias}\right|}{\frac{\theta_{along,beamwidth}}{2}} \tag{39}$$

It should be noted that to simplify the compensation of the beam pattern, spherical coordinates are not used here, but angles in two azimuths are used, and the conversion of the angles in spherical coordinates is expressed as Equation (40).

$$\begin{cases} \theta_{athwart} = arctan2(tan\theta sin\varphi) \\ \theta_{alongship} = arctan2(tan\theta cos\varphi) \end{cases} \tag{40}$$

When calculating the compensation value of the beam pattern, it is only the necessary to us the calculated azimuth angles of the target in two orthogonal directions.

3.4. Copper Ball Broadband TS Measurement

For broadband measurement, the scattering of metal balls is considered simple and ideal, and their frequency response is relatively stable in broadband. By measuring the TS of a standard scattering sphere, the rationality and effectiveness of the TS estimation algorithm can be evaluated [20]. This experiment was conducted in an anechoic pool with length, width and depth of 7 m, 6 m, and 5 m, respectively.

Before the experiment, it was necessary to measure the underwater parameters and the standard scattering sphere parameters and to set the emission signal parameters. The parameters calculated by consulting the literature are shown in Table 5 [21,42].

Table 5. Water parameters, copper ball parameters, and emission signal parameters; some parameters were directly derived from the literature or were calculated according to methods therein.

Parameter	Values
Water Parameters	
Temperature (°C)	23.2
Salinity (‰)	0
Depth (m)	2.0
Density (kg/m^3)	0.9975
Sound velocity (m/s)	1486.5
Copper Parameters	
Material	Copper
Diameter (mm)	63
Density (kg/m^3)	8947
Compressed wave speed	4760
Shearing wave speed	2288.5
Transmit Parameters	
Type	Linear FM
Pulse duration (ms)	1.024
Frequency range (kHz)	160~260
Transmit power (W)	150
Ping interval (ms)	200
Max range (m)	10

The layout of the experimental equipment is shown in Figure 9. The copper ball and transducers were, respectively, loaded onto the traveling vehicle using a rotating function. In order to verify the rationality and effectiveness of the broadband split beam TS algorithm, we set the straight-line distance between the ball and the transducer to 5 m, keeping the distance unchanged, and conducted an axial TS test. This was used to verify the performance of the algorithm without the influence of the beam pattern. The transducer was then rotated at intervals of 1° so that the copper ball was positioned at different angles of the beam pattern to verify the performance of the split-beam positioning algorithm in estimating the intensity of the nonaxial targets.

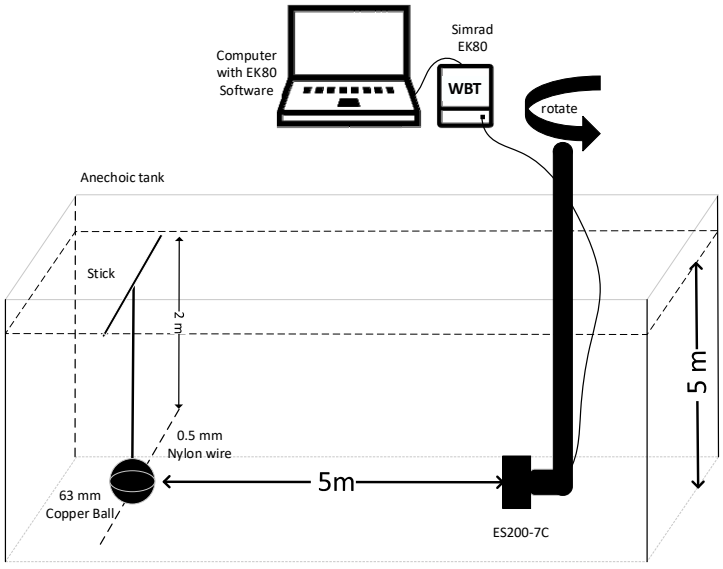

Figure 9. Experimental design for copper ball broadband TS measurement.

We used the algorithm derived in this article to directly estimate the TS of the original split-beam four-channel signal collected by the EK80, obtaining the TS data at different angles and their mean square error at different frequencies in the same image, as shown in Figure 10.

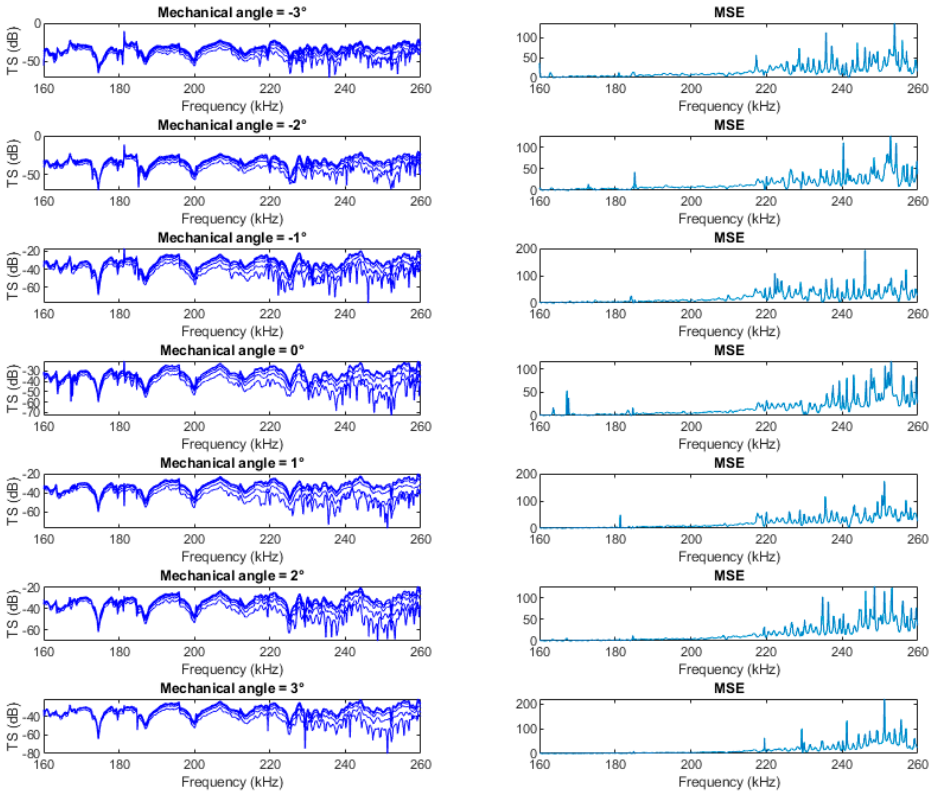

Figure 10. Broadband TS calculation and the corresponding mean square error of the copper spheres at different angles.

It was discovered that in the low-frequency range, the measured datasets were relatively stable, and the data dispersion was low. As the frequency increased, the dispersion of the measured values gradually increased. Similar situations were also reported in the literature [7,12,43].

The reason why these data fluctuate with the frequency may be explained as follows:

1. As the operating frequency of the transducer increases, the sensitivity of the transducer to changes in the surrounding environment increases [44].
2. Under water, the higher the frequency, the shorter the wavelength, and the higher the roughness of the target surface compared to the wavelength. Even for standard spheres, there may be subtle differences in scattering characteristics on different surfaces [5,20].

For point 1, it is assumed that the distribution of the coupled parameters is based on the law of large numbers and the disturbance to the signal occurs in the Gaussian distribution. Multiple pings of the original signals that meet the requirements can be weighted and averaged before broadband TS estimation is performed to obtain values that are closer to the true value [45].

For point 2, The waiting time after any movement operation during the measurement process can be extended, and the smoothness of the surface and the overall shape characteristics of the sphere to be measured can be ensured to meet the standards.

Due to the lack of professional instruments for measuring the differences in copper ball surfaces and the lack of additional tests for copper balls, this paper adopted the first method mentioned above to average the original collected signals.

The standard sphere TS can be calculated from the parameters in Table 5 [46,47]. The EK80 software also provides an estimate of TS during the data collection process. The method described in the article, the EK80 measurement data, and the theoretical TS data of the standard sphere were used for comparison. The results are shown in Figure 11.

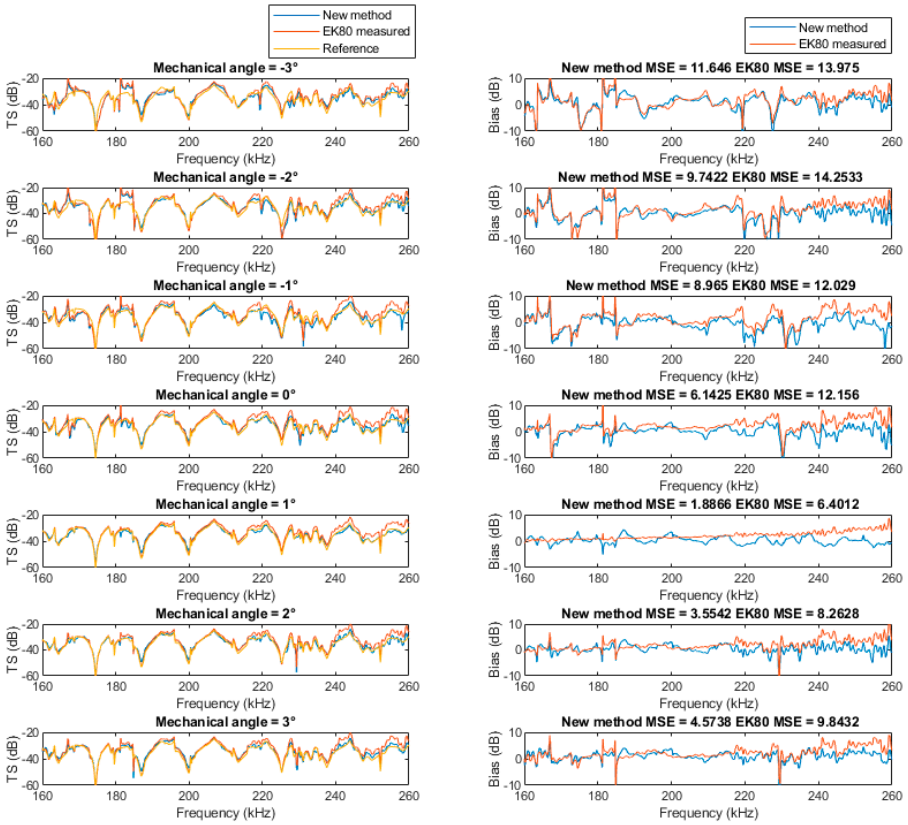

Figure 11. Comparison between the measured and reference values of copper ball broadband TS.

It can be seen that both methods show relatively consistent TS estimation performance, but there is a certain deviation from the standard value. The estimates exhibit smaller deviations in the frequencies from 190 kHz to 220 kHz. Far from the nominal frequency, the deviations are larger and exhibit more fluctuations. The mean square error of the EK80 algorithm is slightly larger than that of the algorithm mentioned in the article. This may be due to the need for recalibration as a long time has passed since the equipment was last calibrated.

4. Discussion

The broadband quantification process for echo signals is much more complicated than that under narrowband conditions, requiring the consideration of more parameters and the use of circuit analysis and complex analysis to complete quantitative analysis [7]. Compared with traditional methods, this method provides a more complete discussion of split beam technology and broadband technology. Although the steps seem more cumbersome and require professional instruments and equipment to measure various parameters of the transducer and medium parameters, the model proposed in the article can theoretically be adapted to all equipment based on split-beam technology or sonar equipment including positioning and power measurement functions. Although the variables are strictly controlled and possible disturbances in the measured values, including digital FIR filtering, matched filtering, and multiple ping data mean filtering, are taken into account, there is still a certain level of error compared to the theoretical value. The main sources of measurement errors are as follows:

1. EK80 did not provide data at the original sampling rate, but instead provided data after two decimations. The equivalent sampling frequency was only 187.5 kHz. When the pulse width is limited, the frequency resolution is low [37], and accurate frequency estimation results of voltage amplitude cannot be provided.
2. Some impedance parameters and sensitivity data are sourced from factory test reports, during long-term use, some changes may occur [5,27], resulting in errors in estimated values at some frequencies.
3. The signal propagation medium is time-varying and will be affected by the physical environment, including weather changes and vehicle shaking, causing fluctuations in the measurement results [48].
4. During long-term use the oxidation and unevenness of the surface become inconsistent with the copper ball in the reference data [20].

Regarding the first point, Jech compared two narrowband devices EK60 and EK500. Compared with EK500, the sampling rate of EK60 decreased, and the smoothness of the calculated TS also decreased [49]. This may be improved by increasing the sampling rate.

Regarding the second point, the transducer will change with the physical conditions. Dealing with time-varying nonlinear systems is complicated. The most effective and simple solution at present is to regularly re-measure the parameters mentioned in the method.

Regarding the third point, one can refer to the acquisition scheme for narrowband echo sounders provided in Ref. [48]. There is less research on broadband, which may be related to the complexity of broadband equipment.

Regarding the fourth point, chemically stable and high-hardness spheres should be used where possible. Chu et al. found that net pockets will affect the sound scattering characteristics [21]. Therefore, it is necessary to ensure that the way the sphere is suspended in the water will not affect the sound scattering characteristics. The production method of a net bag for hanging metal balls can be found in Ref. [5].

The above-mentioned errors are difficult to perfectly solve in the actual measurement process. The increase in sampling rate will incur storage and calculation problems [7]. Parameter calibration requires the use of professional instruments and specific experimental environments for measurement. Judging from the copper ball test results, the error is slightly smaller than that of the built-in algorithm of the EK80 software, which proves the rationality and effectiveness of the method proposed in this article.

From the analysis of the previous demonstration process, this broadband TS calculation method can be applied to any broadband split-beam transducer that can locate targets within the beam. In the field of fishery acoustics, a large number of studies are based on TS. The development of multi-frequency and broadband technologies in recent years has brought new possibilities to TS-based target recognition. At present, due to the particularity and complexity of broadband equipment, many problems remain to be solved before it can be fully promoted and used. It is hoped that the new method proposed in this article can be applied to diverse equipment, and that more acoustic equipment will be available in the future to provide new and valuable enhancements to fishery acoustics.

Author Contributions: Q.A. and H.L. designed the experiment and devised various testing methods; J.T. provided experimental equipment and participated in experimental planning; and J.Y. and C.L. collected data for this experiment. All authors have read and agreed to the published version of the manuscript.

Funding: This research received no external funding.

Institutional Review Board Statement: Not applicable.

Informed Consent Statement: Not applicable.

Data Availability Statement: The data that support the findings of this study are available on request from the first author, Q.A., upon reasonable request.

Acknowledgments: The authors would like to express their sincere thanks to the Institute of Hydroecology, Ministry of Water Resources and Chinese Academy of Sciences, which provided equipment for the experiment. They would also like to thank the Fishery Machinery and Instrument Research Institute. for their contribution to the experimental plan.

Conflicts of Interest: The authors declare no conflict of interest.

Appendix A

The names, symbols, and units of physical quantities must be precisely defined to ensure effective scientific communication. However, different fields of study, such as physics, electrical engineering, radar, and sonar, often use different terms and symbols, and the same symbols can be used for different items, even within the same field. In summary, scientists and researchers often exhibit preferences for specific terms and symbols. The following terminology is mainly based on the suggestions of MacLennan [50] and follows the SI units. A symbol should uniquely represent a term.

For the convenience of reading, the following table lists each variable in the formula in section order, with a brief explanation.

Table A1. Symbols, units, and descriptions for Section 2.1.

Symbol	Unit	Description
ρ_w	kg/m^3	Density of water
u_0	m/s	Particle vibration speed
a	m	Transducer diameter
k	rad/m	Wave number
c_w	m/s	Underwater sound speed
α	dB/m	Absorption coefficient
$p(r,\theta)$	Pa	The sound pressure of the transducer at any position in the field
r	m	Distance from the equivalent sound center of the transducer
p_0	Pa	Axial sound pressure amplitude at the transducer reference distance
p_{bs0}	Pa	Backscattering sound pressure at reference distance from scatterer
$b(\theta)$	None	Transducer beam pattern
p_{bs}	Pa	Scattered sound pressure at transducer reference distance
σ_{bs}	m^2	Backscattering cross section
TS	dB re $1m^2$	Target strength

Table A2. Symbols, units, and descriptions for Section 2.2.

Symbol	Unit	Description
s_u	1 μPa/V@1m	Axial emission voltage sensitivity at reference distance
m_u	1V/μPa @1m	Axial received voltage sensitivity at reference distance
p_{ax}	Pa	Equivalent axial sound pressure
V_o	V	Open-circuit voltage when the transducer is receiving
V_T	V	The voltage loaded across the transducer in the transmitting state
V_R	V	The sampling voltage of the sampling circuit in the receiving state
Π_T	W	Transmit power
Z_T	Ω	Transducer impedance
R_T	Ω	Transducer resistance
Z_E	Ω	Receiver circuit impedance
R_E	Ω	Receiver circuit resistance
F_{Impe}	Ω^{-1}	Impedance factor
Su	dB re 1 μPa/V@1m	Logarithmic representation of transmitted voltage sensitivity
Mu	dB re 1V/μPa @1m	Logarithmic representation of received voltage sensitivity

Table A3. Symbols, units, and descriptions for Section 2.3.

Symbol	Unit	Description
$v(t)$	V	Assumed target echo voltage function
Π_{ref}	W	Assumed target echo power
$s_{ideal}(t)$	None	Ideal wideband signal in time domain
$S(f)$	None	Ideal wideband signal in frequency domain
t	s	Time variables in continuous time domain
T	s	Single frequency signal period
τ	s	Integration time variable
f *or* f_i, f_n	Hz	The signal frequency in the discrete frequency domain
F_{band}	Hz	Broadband signal bandwidth
n	None	Sequence index under time domain discretization
N	None	Finite sequence length under time domain discretization
A_n, A_i *or* C_i	None	Corresponding amplitude in time domain or frequency domain
x, y *etc*	None	Intermediate variable sequence during derivation in time domain
$X_{responsor}(f)$	None	Intermediate variable sequence during derivation in frequency domain
$V_{norm}[n]$	None	Normalized reference voltage discrete sequence
$V_{ref}[n]$	None	Reference voltage discrete sequence

References

1. Orduna Martín, C.; Encina Encina, L.; Rodríguez Ruiz, A.; Rodríguez Sánchez, V. Testing of New Sampling Methods and Estimation of Size Structure of Sea Bass (*Dicentrarchus labrax*) in Aquaculture Farms Using Horizontal Hydroacoustics. *Aquaculture* **2021**, *545*, 737242. [CrossRef]
2. Muhammad, Z.L. Acoustic Systems (Split Beam Echo Sounder) to Determine Abundance of Fish in Marine Fisheries. *Ocean. Fish.* **2017**, *3*, 555607. [CrossRef]
3. Foote, K.G.; Traynor, J.J. Comparison of Walleye Pollock Target Strength Estimates Determined from in Situ Measurements and Calculations Based on Swimbladder Form. *J. Acoust. Soc. Am.* **1988**, *83*, 9–17. [CrossRef]
4. Kang, M. Overview of the Applications of Hydroacoustic Methods in South Korea and Fish Abundance Estimation Methods. *Fish. Aquat. Sci.* **2014**, *17*, 369–376. [CrossRef]
5. Demer, D.A.; Berger, L.; Bernasconi, M.; Bethke, E.; Boswell, K.; Chu, D.; Domokos, R.; Dunford, A.; Fassler, S.; Gauthier, S. Calibration of acoustic instruments. In *ICES Cooperative Research Report*; ICES: Copenhagen, Denmark, 2015; Volume 326, 136p. [CrossRef]
6. Traynor, J.J. Fish and Standard-Sphere Targetstrength Measurements Obtained with a Dual-Beam and Split-Beam Echo Sounding System. *Rapp. P.-v. Reun. Cons. Int. Explor. Mer.* **1990**, *189*, 325–335.
7. Andersen, L.N.; Chu, D.; Heimvoll, H.; Korneliussen, R.; Macaulay, G.J.; Ona, E. Quantitative Processing of Broadband Data as Implemented in a Scientific Splitbeam Echosounder. *arXiv* **2021**, arXiv:2104.07248. [CrossRef]
8. Dragesund, O.; Olsen, S. *On the Possibility of Estimating Year-Class Strength by Measuring Echo-Abundance of 0-Group Fish*; ICES: Copenhagen, Denmark, 1965; Volume 13, pp. 44–75.
9. Jurvelius, J.; Marjomäki, T.J.; Peltonen, H.; Degtev, A.; Bergstrand, E.; Enderlein, O.; Auvinen, H. Fish Density and Target Strength Distribution of Single Fish Echoes in Varying Light Conditions with Single and Split Beam Echosounding and Trawling. *Hydrobiologia* **2016**, *780*, 113–124. [CrossRef]
10. Quazi, A. An Overview on the Time Delay Estimate in Active and Passive Systems for Target Localization. *IEEE Trans. Acoust. Speech Signal Process.* **1981**, *29*, 527–533. [CrossRef]
11. Lunde, P.; Korneliussen, R.J. Power-Budget Equations and Calibration Factors for Fish Abundance Estimation Using Scientific Echo Sounder and Sonar Systems. *J. Mar. Sci. Eng.* **2016**, *4*, 43. [CrossRef]
12. Demer, D.A.; Andersen, L.N.; Bassett, C.; Berger, L.; Chu, D.; Condiotty, J.; Hutton, B.; Korneliussen, R.; Bouffant, N.L.; Macaulay, G. *2016 USA–Norway EK80 Workshop Report: Evaluation of a Wideband Echosounder for Fisheries and Marine Ecosystem Science*; ICES Cooperative Research Reports (CRR); ICES: Copenhagen, Denmark, 2017; Volume 336. [CrossRef]
13. Rautureau, C.; Goulon, C.; Guillard, J. In Situ TS Detections Using Two Generations of Echo-Sounder, EK60 and EK80: The Continuity of Fishery Acoustic Data in Lakes. *Fish. Res.* **2022**, *249*, 106237. [CrossRef]
14. Simrad EK500 Operator Manual. Available online: https://www.kongsberg.com/maritime/support/simradsupport/simrad-docs/discontinued-echo-sounders/simrad-ek500/ (accessed on 21 December 2023).
15. Ishimaru, A. Theory and Application of Wave Propagation and Scattering in Random Media. *Proc. IEEE* **1977**, *65*, 1030–1061. [CrossRef]
16. Hao, C.; Orlando, D.; Liu, J.; Yin, C. Introduction to Radar Systems. In *Advances in Adaptive Radar Detection and Range Estimation*; Springer: Berlin/Heidelberg, Germany, 2022; ISBN 9789811663987.

17. Bjørnø, L. Chapter 5—Scattering of Sound. In *Applied Underwater Acoustics*; Neighbors, T.H., Bradley, D., Eds.; Elsevier: Amsterdam, The Netherlands, 2017; pp. 297–362.
18. Yang, Y.; Gastauer, S.; Proud, R.; Mangeni-Sande, R.; Everson, I.; Kayanda, R.J.; Brierley, A.S. Modelling and in Situ Observation of Broadband Acoustic Scattering from the Silver Cyprinid (*Rastrineobola argentea*) in Lake Victoria, East Africa. *ICES J. Mar. Sci.* **2023**. [CrossRef]
19. Stanton, T.K.; Chu, D. Calibration of Broadband Active Acoustic Systems Using a Single Standard Spherical Target. *J. Acoust. Soc. Am.* **2008**, *124*, 128–136. [CrossRef] [PubMed]
20. Hobaek, H.; Forland, T.N. Characterization of Target Spheres for Broad-Band Calibration of Acoustic Systems. *Acta Acust. United Acust.* **2013**, *99*, 465–476. [CrossRef]
21. Chu, D.; Eastland, G.C. Calibration of a Broadband Acoustic Transducer with a Standard Spherical Target in the near Field. *J. Acoust. Soc. Am.* **2015**, *137*, 2148–2157. [CrossRef] [PubMed]
22. Lavery, A.C.; Chu, D.; Moum, J.N. Measurements of Acoustic Scattering from Zooplankton and Oceanic Microstructure Using a Broadband Echosounder. *ICES J. Mar. Sci.* **2010**, *67*, 379–394. [CrossRef]
23. Butler, J.L.; Sherman, C.H. Chapter 5—Transducers as Projectors. In *Transducers and Arrays for Underwater Sound Compress*; Springer: Berlin/Heidelberg, Germany, 2016; pp. 185–272.
24. Lunde, P. Finite-Amplitude Power Budget Equations for Acoustic Fish Abundance Estimation. *J. Mar. Sci. Eng.* **2020**, *8*, 98. [CrossRef]
25. Butler, J.L.; Sherman, C.H. Chapter 10—Acoustic Radiation from Transducers. In *Transducers and Arrays for Underwater Sound Compress*; Springer: Berlin/Heidelberg, Germany, 2016; pp. 517–551.
26. Medwin, H.; Clay, C.S. Chapter 7—Sound Scattered by a Body. In *Fundamentals of Acoustical Oceanography*; Medwin, H., Clay, C.S., Eds.; Applications of Modern Acoustics; Academic Press: San Diego, CA, USA, 1998; pp. 234–286.
27. Demer, D.A.; Renfree, J.S. Variations in Echosounder–Transducer Performance with Water Temperature. *ICES J. Mar. Sci.* **2008**, *65*, 1021–1035. [CrossRef]
28. Butler, J.L.; Sherman, C.H. Chapter 6—Transducers as Hydrophones. In *Transducers and Arrays for Underwater Sound Compress*; Springer: Berlin/Heidelberg, Germany, 2016; pp. 281–341.
29. Wang, Y.; Sun, D.; Yong, J. Design of Broadband Matching Circuit for Underwater Acoustic Communication Transducer. In Proceedings of the 2015 International Conference on Intelligent Systems Research and Mechatronics Engineering, Zhengzhou, China, 11–13 April 2015; Atlantis Press: Amsterdam, The Netherlands, 2015; pp. 2298–2305.
30. Xiao, D.; Fan, Q.; Xu, C.; Zhang, X. Measurement Methods of Ultrasonic Transducer Sensitivity. *Ultrasonics* **2016**, *68*, 150–154. [CrossRef]
31. Soliveres, E.; Poveda, P.; Estruch, V.D.; Pérez-Arjona, I.; Puig, V.; Ordóñez, P.; Ramis, J.; Espinosa, V. Monitoring Fish Weight Using Pulse-Echo Waveform Metrics. *Aquac. Eng.* **2017**, *77*, 125–131. [CrossRef]
32. Puig-Pons, V.; Muñoz-Benavent, P.; Pérez-Arjona, I.; Ladino, A.; Llorens-Escrich, S.; Andreu-García, G.; Valiente-González, J.M.; Atienza-Vanacloig, V.; Ordoñez-Cebrian, P.; Pastor-Gimeno, J.I. Estimation of Bluefin Tuna (*Thunnus thynnus*) Mean Length in Sea Cages by Acoustical Means. *Appl. Acoust.* **2022**, *197*, 108960. [CrossRef]
33. Kubilius, R.; Bergès, B.; Macaulay, G.J. Remote Acoustic Sizing of Tethered Fish Using Broadband Acoustics. *Fish. Res.* **2023**, *260*, 106585. [CrossRef]
34. Oppenheim, A.V.; Willsky, A.S.; Nawab, S.H.; Ding, J.-J. Chapter 3—Fourier Series Representation of Periodic Signals. In *Signals and Systems*; Prentice Hall: Upper Saddle River, NJ, USA, 1997; pp. 177–250.
35. Liu, D.; Qu, H.; Wang, W.; Deng, J. Multiple Targets Detection of Linear Frequency-Modulated Continuous Wave Active Sonar Using Fractional Fourier Transform. *Integr. Ferroelectr.* **2020**, *209*, 1–10. [CrossRef]
36. Guo, Y.; Yang, L. Method for Parameter Estimation of LFM Signal and Its Application. *IET Signal Process.* **2019**, *13*, 538–543. [CrossRef]
37. Oppenheim, A.V.; Willsky, A.S.; Nawab, S.H.; Ding, J.-J. Chapter 5—The Discrete-Time Fourier Transform. In *Signals and Systems*; Prentice Hall: Upper Saddle River, NJ, USA, 1997; pp. 358–396.
38. Levanon, N.; Mozeson, E. Chapter 2—Matched Filter. In *Radar Signals*; John Wiley & Sons: Hoboken, NJ, USA, 2004; pp. 20–33.
39. Oppenheim, A.V.; Willsky, A.S.; Nawab, S.H.; Ding, J.-J. Chapter 6—Time and Frequency Characterization of Signals and Systems. In *Signals and Systems-6*; Prentice Hall: Upper Saddle River, NJ, USA, 1997; pp. 423–472.
40. Simrad ES200-7C. Available online: https://www.kongsberg.com/maritime/products/commercial-fisheries/td/200-khz/simrad-es200-7c/ (accessed on 20 December 2023).
41. Li, J.; Jiang, L.; Yu, F.; Zhang, Y.; Gao, K. Research on Improving Measurement Accuracy of Acoustic Transfer Function of Underwater Vehicle. In *MATEC Web of Conferences*; EDP Sciences: Les Ulis, France, 2021; Volume 336, p. 01006. [CrossRef]
42. Ainslie, M.A.; McColm, J.G. A Simplified Formula for Viscous and Chemical Absorption in Sea Water. *J. Acoust. Soc. Am.* **1998**, *103*, 1671–1672. [CrossRef]
43. Conti, S.G.; Demer, D.A. Wide-Bandwidth Acoustical Characterization of Anchovy and Sardine from Reverberation Measurements in an Echoic Tank. *ICES J. Mar. Sci.* **2003**, *60*, 617–624. [CrossRef]
44. Au, W.W.; Benoit-Bird, K.J. Broadband Backscatter from Individual Hawaiian Mesopelagic Boundary Community Animals with Implications for Spinner Dolphin Foraging. *J. Acoust. Soc. Am.* **2008**, *123*, 2884–2894. [CrossRef]

45. De Robertis, A.; Higginbottom, I. A Post-Processing Technique to Estimate the Signal-to-Noise Ratio and Remove Echosounder Background Noise. *ICES J. Mar. Sci.* **2007**, *64*, 1282–1291. [CrossRef]
46. Demer, D.A.; Conti, S.G.; De Rosny, J.; Roux, P. Absolute Measurements of Total Target Strength from Reverberation in a Cavity. *J. Acoust. Soc. Am.* **2003**, *113*, 1387–1394. [CrossRef]
47. Maclennan, D.N. The Theory of Solid Spheres as Sonar Calibration Targets. *Scottish Fish. Res. Rep.* **1981**, *22*, 1–16.
48. Jech, J.M.; Schaber, M.; Cox, M.; Escobar-Flores, P.; Gastauer, S.; Haris, K.; Horne, J.; Jarvis, T.; Ladroit, Y.; O'Driscoll, R. Collecting Quality Echosounder Data in Inclement Weather. In *ICES Cooperative Research Report*; ICES: Copenhagen, Denmark, 2021; Volume 352, 108p. [CrossRef]
49. Jech, J.M.; Foote, K.G.; Chu, D.; Hufnagle Jr, L.C. Comparing Two 38-kHz Scientific Echosounders. *ICES J. Mar. Sci.* **2005**, *62*, 1168–1179. [CrossRef]
50. MacLennan, D.N.; Fernandes, P.G.; Dalen, J. A Consistent Approach to Definitions and Symbols in Fisheries Acoustics. *ICES J. Mar. Sci.* **2002**, *59*, 365–369. [CrossRef]